Front. Med. 2025, 19(6): 1269−1282
https://doi.org/10.1007/s11684-025-1167-x

RESEARCH ARTICLE

Sub-threshold depolarization differentially regulated by multiple ion channels plays a key role in initiation of baroreflex afferent neurotransmission evidenced from baroreceptor terminals to its cell bodies

Yinzhi Xu[1,*], Zhaoyuan Xu[1,*], Huixiao Fu[1], Mao Yue[1], Jiaqun Li[1], Changpeng Cui[1], Xuelian Li[1], Xianghui Kong[2], Baiyan Li (✉)[1]

[1]*State Key Laboratory of Frigid Zone Cardiovascular Diseases (SKLFZCD), Department of Pharmacology (State Key Laboratory-Province Key Laboratories of Biomedicine-Pharmaceutics of China, Key Laboratory of Cardiovascular Research, Ministry of Education), College of Pharmacy, Harbin Medical University, Harbin 150081, China;* [2]*Institute of Microbiology, Heilongjiang Academy of Sciences, Harbin 150010, China*

Abstract **Direct evidence regarding ion channel-mediated initiation of baroreflex/visceral neurotransmission remains limited. Here, aortic-arch, vagus-nodose slice, and isolated neurons were employed with single-fiber/whole-cell patch-clamp recordings to record instantaneous discharge of the aortic depressor nerve, spontaneous/evoked membrane depolarizations under different pharmacological interventions. Strikingly, profiles of A-fiber's instantaneous firing frequency (IFF), including pressure threshold, rate, and sensitivity, were significantly reduced by 10 μmol/L flufenamic acid (FAA) and further suppressed by 3 μmol/L GsMTx4. Conversely, 3 μmol/L Yoda1-enhanced IFF was reversed by GsMTx4 and partially inhibited by FAA, consistent with step depolarization-evoked action potentials (APs). In < 10% of A-type neurons, spontaneous APs accompanied by major (Ma-STPs) and minor sub-threshold depolarizations (Mi-STPs) were abolished by nanomolar tetrodotoxin. FAA only blocked spontaneous APs, while GsMTx4 suppressed both APs and Ma-STPs. The equal number of APs and Ma-STPs before and after FAA suggests that spontaneous APs initiate from Ma-STPs. Further, single-cell transcriptomic analysis revealed significant *Piezo1* and *TRPM4* co-expression in neurons. Gene co-expression and clustering analysis support their cooperative role in the baroreflex and visceral afferent pathways, validated by gene expression data. These findings demonstrate that TTX-sensitive Na^+ (TTX-S), *Piezo1*, and *TRPM4* channels each possess important intrinsic functions and play unique roles in the initiation of baroreflex/visceral neurotransmission.**

Keywords instantaneous discharge; aortic depressor nerve; aortic arch; action potential; visceral sensory neurons; TTX-sensitive Na^+/*Piezos*/*TRPM4* channel; sub-threshold depolarization

Introduction

Baroreflex is an important mechanism by which the central nervous system (CNS) controls blood pressure (BP) in response to acute fluctuations [1] due to changes in posture, exercise, stress, drugs, and other stimuli. The baroreflex is initiated by pressure receptors (mechanoreceptors) located within the walls of aorta, in which aortic baroreceptor terminals are located close to the apex of aortic arch, between the left common carotid and left subclavian arteries, and their axons form a nerve bundle called aortic depressor nerve (ADN) [2]. In human, ADN joins the vagus nerve right after rising from the aortic arch. However, in rats and rabbits, the ADN does not join the vagus nerve until close to the nodose ganglion (NG) [3], so they are ideal animals for studying the pressure encoding of aortic baroreceptor, baroreceptor neurons, and the baroreflex afferent function.

Mechanical deformation of the vessel wall elicited by an increase in BP is transduced/encoded into a train of

Received March 20, 2025; accepted August 4, 2025

Correspondence: Baiyan Li, liby@ems.hrbmu.edu.cn

*These authors contributed equally to this work.

action potentials (APs) that is frequency-modulated. This signal is raised from the terminals in the aorta, transmitted to their cell bodies within the NG, and then relayed via sensory fibers into the nucleus tractus solitarius (NTS) [4,5] in the brainstem through one-on-one connection, where these signals are processed and integrated with other visceral neural information from other organs/systems including the heart, circulation, gastrointestinal, respiratory, etc. Even though these conceptions have been well established based upon the experimental investigations, the direct evidence regarding the exact roles and collaborative mechanism among mechanosensitive channels, particularly for *Piezo1* [2] and *TRPM4* [6], as well as voltage-gated sodium channels [7] in an initiation of baroreflex/visceral afferent neurotransmission [8] are very limited due presumably to technical reasons, appropriate animal models, or the lack of selective agonist/antagonist for those channels. In this study, instantaneous discharge of a single-fiber of ADN from aortic arch preparation along with spontaneous or evoked discharge of APs from NG neurons isolated from adult rats were selected to investigate discharge profiles before and after treatments. These observations provide the first line of evidence showing that TTX-S, *Piezo1*, and *TRPM4* channels play unique role in an initiation and orchestration [9] of baroreflex/visceral afferent neurotransmission, and the major sub-threshold depolarization (Ma-STPs) [10,11] mediated by *Piezo1* is a key player in initiating discharge of baroreceptor terminals, which adds additional knowledge in the field regarding these channels for fully understanding their functions under physiologic and pathophysiological conditions and future perspective of their pharmacological potentials [12,13].

Materials and methods

Animals

Adult male Sprague-Dawley (SD) rats were purchased from the Experimental Animal Facility of the 2nd Affiliated Hospital (Laboratory Animal Certificate Number: SCXK (Hei) 2019-001, grade II) of Harbin Medical University and maintained in our animal facility for at least one week before use. The rats were maintained in a pathogen-free environment, at a temperature of 21–23 °C, housed 5 per cage, under a 12-h light/dark cycle, and were provided with standard rodent chow and water *ad libitum*. All protocols for animals used in these experiments were consistent with the recommendations of the American Veterinary Medical Association Euthanasia Panel and the National Institutes of Health publication "Guide for the Care and Use of Laboratory Animals," and approved by Harbin Medical University Institutional Animal Care and Use Committee.

Chemicals

Yoda1 (#HY-18723) and GsMTx4 (#HY-P1410) were purchased from MedChem Express (Monmouth Junction, NJ, USA); flufenamic acid (FAA, #F9005), capsaicin (Cap, #404864) and sodium nitroprusside (NP, #228710) were purchased from Sigma (St. Louis, MO, USA). Stock solutions of the drugs were prepared in appropriate solvents, kept at −80°C, and diluted in recording solution prior to use. All other chemicals for neuron isolation and recording solutions, as well as enzymes required for neuronal dissociation, were from standard commercial sources.

Aortic arch preparation

Young male SD rats weighing 100 g about 4-week age were used for the aortic arch preparation according to the procedures previously described [2,14]. Briefly, after the rats were completely anesthetized with sodium isopentobarbital (3%, 25 mg/kg, i.p.) and surgical procedures were performed, the electrode was carefully placed onto the ADN and both were moved upward slightly into the layer of mineral oil covered on the surface of warm Krebs-Henseleit bicarbonate buffer (37 °C; bathing medium) containing (in mmol/L): 118 NaCl, 4.7 KCl, 1.25 $CaCl_2$, 1.2 $MgSO_4$, 1.2 KH_2PO_4, 25 $NaHCO_3$, and 11.1 glucose, bubbled with 5% CO_2-95% O_2. A computer-controlled pressure ramp (Fig. S1B) was initiated, and pressure-dependent discharge (Fig. S1A) was recorded before and after treatments from a single A-fiber identified by discharge characteristics and insensitive to 100 nmol/L Cap. Discharge capability was quantified as instantaneous firing frequency (IFF) (Fig. S1C) characterized by pressure threshold (Pth), frequency threshold (Fth), and sensitivity (Sth)/slope [15]. To eliminate potential vascular effects of aorta with attached branches and discharge activity from unmyelinated C-fiber afferents, Cap and SNP were added to the pressure solution.

Nodose ganglia slice preparation

Adult male SD rats weighing 220–250 g were selected for the nodose slice preparation as previously described [16,17]. Briefly, after the rats were completely anesthetized, the left side of NG with entire vagus nerve was carefully dissected and placed in chilled (4–8 °C) recording solution (see below) to remove the connective tissue surrounding, and transferred into enzymatic solution. After that, enzymatic solution was replaced by the recording solution and then the slice was transferred into the recording chamber for at least 1 h for ion channel recovery from enzymatic isolation before the patch-clamp recording.

Isolated neurons preparation

The procedures for isolated preparation used for electrophysiological studies were described in our earlier publications and were only briefly described here [16–18]. After enzymatic treatments, the enzyme solution consisting of 10 U/mL of Papain (Worthington, Lakewood, NJ), followed by 1.0 mg/mL of type II Collagenase and 2.5 mg/mL of Dispase (Roche, USA) was then replaced with nodose complete medium consisting of 90 mL of DME-F-12 medium (Sigma, St. Louis, MO), 5.0 mL of Fetal Bovine Serum (Hyclone, Logan UT), 1.0 mL of Penicillin-Streptomycin (Invitrogen, Grand Island, NY), and 100 μmol/L of MITO + Serum Extender (Collaborative Res, Bedford MA), and the NG was triturated with an aspiration pipette to dissociate the cell bodies for plating onto a poly-D-lysine (0.5 mg/mL aqueous solution)-coated coverslip. The isolated NG neurons were maintained in an incubation chamber (5% CO_2-95% air) at 37 °C for at least 4 h and the recordings were performed within 8 h after isolation.

Vagus-nodose slice preparation

The procedures were described in detail previously (#16). Briefly, the NG and vagus nerve were suspended in a gel block prepared using low gelling temperature agarose (1.5%, Sigma, A2576) with recording media (see above) and the temperature was monitored using a digital thermometer, which ensured the NG was mounted in a viscous solution that was cool enough for live tissue (34–35 °C). After rapidly solidifying the agarose in a freezer (20 °C, 1 min), the gel block was trimmed under stereomicroscopy and the gel section was then mounted onto a tissue block using a cynoacrylate adhesive and immersed in the slicing basin filled with an ice/liquid mixture of recording solution. By utilizing a vibrating blade microtome (Leica, VT1000S), the microtome was adjusted for maximum blade translation and slow advancement speed (0.05–0.5 mm/s). Then, 50–100 μm thick slices were finally cut. A glass coverslip was used to lift out the thin slice of agarose containing the ganglion-nerve preparation, which was then placed into a petri dish filled with an enzymatic solution (see below).

Afferent fiber-type identification

First, in the arch preparation, all recorded IFFs originated from myelinated A-type fibers since 100 nmol/L Cap was included in the pressure solution, which selectively blocked the activity of all unmyelinated C-type fibers [15]. Second, in the vagus-nodose slice preparation, a conduction velocity (CV) (Fig. S2A) was used to identify the fiber-type of tested neurons, in conjunction with phase plot (Fig. S2B). The CV of A-type fibers is always greater than 10 m/s at room temperature [19]. Third, for isolated neurons, a set of waveform characteristics, including AP firing threshold < −40 mV, APD_{50} < 1.0 ms, maximal up-stroke (UV_{MAX}) > 250 mV/ms, and down stroke velocity (DV_{MAX}) > 100 mV/ms, were used to classify the A-type fiber-type of tested neurons conjugated with the absence of a repolarization hump, verified using phase plots (Fig. S3A–S3C) or no response to 100 nmol/L Cap applied at the end of recording [17].

Electrophysiology

The protocol and solutions for the whole-cell current-clamp techniques used in this study were described in detail previously [16,17]. Briefly, four current protocols were implemented using an Axoclamp 700A (Axon Instruments, Scottsdale, AZ, USA). First, brief constant current pulses of sufficient magnitude (⩽500 ms, ⩾400 pA) to elicit a single AP for fiber-type identification in isolated neurons. Second, step currents (500–1000 ms, 5–300 pA) were applied to assess the repetitive discharge. Third, a gap-free protocol with varying durations was used to examine spontaneous discharge/current-clamp mode or spontaneous inward currents/voltage-clamp mode after tight seal/ruptured patch. Fourth, short-duration (⩽ 200 ms) monophasic constant current pulse was applied to the vagus nerve using a platinum (90%)/iridium (10%) bipolar electrode (2 mm spacing of 3 mm uninsulated tips). The cathode was positioned a measured distance (1–1.5 cm) from the center of the NG. Since the stimulus artifact was generally kept below 0.5 ms, CV approaching 30 m/s could theoretically be resolved with a 1.5 cm nerve length. The stimulus intensity was increased by about 20% beyond the threshold for activation. For all current-clamp recordings, patch pipettes (7052, Corning) were pulled (P-87, Sutter) and polished (MF-830, Narishige) down to a resistance of 1–1.5 MΩ and after ruptured patch the bridge balance was adjusted to avoid partial rupture or resealing during recording. All data were low-pass filtered to 10 kHz and digitized at a sampling rate of 40 kHz. Experimental protocols and data collection were conducted using the Digidata 1440A controlled by pCLAMP v10.3 (Molecular Devices; Sunnyvale, CA, USA) operating on a PC platform at room temperature (21–23 °C).

For recording of AP/whole-cell current-clamp recordings, the extracellular solution consisted of (in mmol/L): 137 NaCl, 5.4 KCl, 1.0 $MgCl_2$, 2.0 $CaCl_2$, 10 glucose, 10 N-2-hydroxyethylpiperazine-N'-2-ethane-sulfonic acid (HEPES), and the pipette solution consisted of (in mmol/L): 10 NaCl, 50.0 KCl, 50 K_2SO_4, 5.0 $MgCl_2$, and 10 HEPES. The pH for pipette and bath solutions was adjusted to 7.25 and 7.35 using 1 mol/L KOH and 1 mol/L NaOH. Osmolarity of the extracellular

and intracellular solutions was adjusted to 310–315 mOsm/L and 290–295 mOsm/L, respectively, using D-Manitol (Sigma, MO, USA).

qRT-PCR

The tissue of the NG was collected from 2 rats as one sample and qRT-PCR was performed according to the protocol provided by the manufacturer. Briefly, the TRIzol reagent (#15596026, Invitrogen) was used to extract total RNA and cDNA synthesis was performed via reverse transcription, followed by quantitative PCR amplification using SYBR Green on ABI QuantStudio™ 6 Flex RT-PCR system (#4485691, Applied Biosystems, Woodlands, Singapore) with *Piezo1*, *TRPM4*, and β-*tubulin* primers. *Piezo1* sense: GACGCCTCACAAGGAA-AGC, *Piezo1* anti-sense: GGGCAGCATCTATGTCATCC, *TRPM4* sense: GCACTTCCGTGTCTGTCTCT, *TRPM4* anti-sense: AGTCGCTGTCTCGCTTGTC. Data of relative gene expression were analyzed with $2^{-\Delta\Delta Ct}$ method.

Bioinformatics data analysis

Use Tabula Sapiens database to plot cell annotation subgroup figure, visualize the expression distribution figure of *Piezo1* and *TRPM4* respectively. Expression data for all cells, including nerve cells, were downloaded from the Tabula Sapiens database. Additionally, transcriptomic data sets GSE233733 (vagus nerve sequencing data from COVID-19 patients) and GSE43490 (vagus dorsal nucleus sequencing data) were obtained from the GEO database. While the microarray sequencing data of cells in the brain were retrieved from the Allen Brain Map database.

Pearson correlation analysis was performed using Prism 10 to evaluate the relationship between *Piezo1* and *TRPM4* expression levels. A significance threshold of $P < 0.05$ was applied. Correlation coefficients were interpreted as follows: $r > 0$ indicates a positive correlation, and $r > 0.5$ indicates a strong positive correlation.

Data acquisition and statistical analysis

Statistical analysis and figure generation were performed using Excel v2007 and Origin v7.0 (OriginLab, Northampton, MA, USA). All electrophysiological data generated by patch-clamp recordings were analyzed with Clampfit (v10.3, Molecular Devices; Sunnyvale, CA, USA). Statistical analyses were only performed on studies that had at least 3 complete observations ($n \geqslant 3$), as indicated in the main text of figure legends. Both paired (before and after drug application in the same group) and unpaired (between different groups) Student's *t*-tests were employed to assess the statistical significance. When necessary, one-way ANOVA with post-hoc Tukey test was utilized for comparisons among multiple data sets. The averaged data are presented as mean ± standard deviation (SD). A *P* value of less than 0.05 was considered statistically significant.

Results

Instantaneous discharge of single-fiber recording in aortic arch preparation with *Piezo1* or *TRPM4* channel manipulation

Growing evidence suggests that *Piezo1*/*TRPM4* channels function as mechanosensors involved in initiating baroreflex afferent neurotransmission at the baroreceptor terminals of the aortic arch. However, direct evidence is lacking. Here, an instantaneous discharge of single-fiber (Fig. S1) from the ADN using *in situ* aortic arch preparation was monitored before and after FAA, a selective blocker for *TRPM4*, or GsMTx4, a selective blocker for *Piezo1* (Fig. 1). To selectively analyze A-type afferents, exclude potential C-fiber discharge, and eliminate vascular effects, 100 nmol/L Cap and 300 nmol/L SNP were included in the pressure solution. The results demonstrated that 10 μmol/L FAA significantly reduced IFF and that was further suppressed by subsequent application of 3 μmol/L GsMTx4 on top of FAA (Fig. 1A), suggesting that both *TRPM4* and *Piezo1* contribute to afferent signaling. Meanwhile, those parameters for characterizing the profiles of IFF, such as the Pth, Fth, and sensitivity (slope), were analyzed and these results clearly demonstrated that both Pth (Fig. 1B) and Fth (Fig. 1C) were consistently well with the arch recordings, whereas, in the case of sensitivity (Sth)/slope, it was not altered by 10 μmol/L FAA and further downgraded by GsMTx4, but the control level of sensitivity could dramatically be reduced in the presence of 3 μmol/L GsMTx4 (Fig. 1D). These *in situ* observations using the aortic arch preparation with single-fiber recording highly suggest that *Piezo1*/*TRPM4* are two key intrinsic players in initiating baroreflex afferent neurotransmission under physiologic condition.

Our previous patch-clamp data have shown that the firing frequency of NG neurons isolated from adult rats can be elevated by 3 μmol/L Yoda1 [2], whether exogenous *Piezo1* agonist can also raise the IFF in the aortic arch preparation would be essential to evaluate the pharmacological potential for *Piezo1* activation. To answer this particular question, 3 μmol/L Yoda1 was applied into the pressure solution. As expected, the resting level of IFF was obviously enhanced by Yoda1, and this effect was completely abolished by subsequent application of 3 μmol/L GsMTx4 (Fig. 2A). Furthermore,

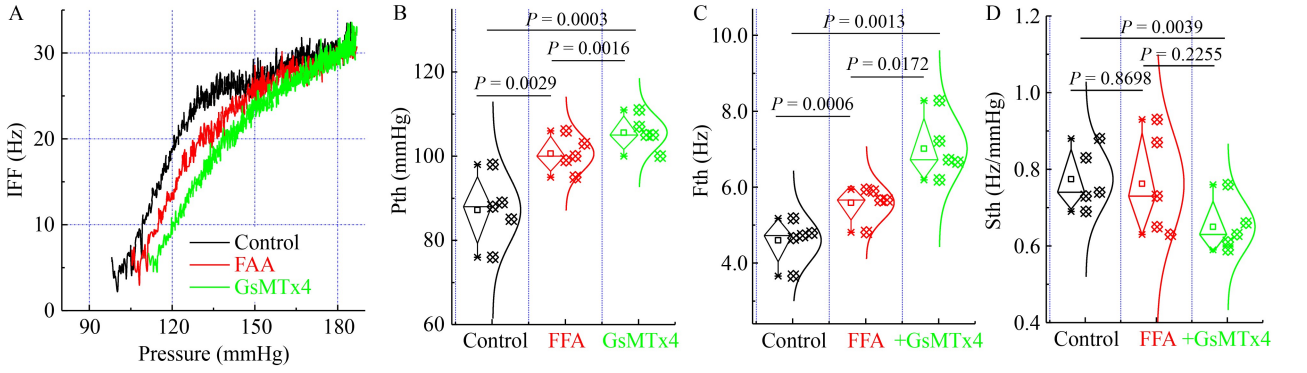

Fig. 1 Changes in profiles of IFF including thresholds for pressure (Pth), frequency (Fth), and sensitivity (Sth, slope) of single-fiber discharge recorded from ADN in the presence of FAA (blocker for *TRPM4*) or GsMTx4 (blocker for *Piezo1*). (A) Representative recordings of instantaneous discharge of myelinated A-type single-fiber before (DMSO as control), and after FAA (10 μmol/L, red) or GsMTx4 (3 μmol/L, green). 100 nmol/L Cap and 100 nmol/L sodium nitroprusside were included in the solution for the pressure ramp to distinguish A-fiber and remove possible discharge from C-fiber as well as vascular effect. (B–D) Averaged data for Pth, Fth, and Sth before and after treatments. Summarized data were presented as mean ± SD, $n = 5$ complete recordings.

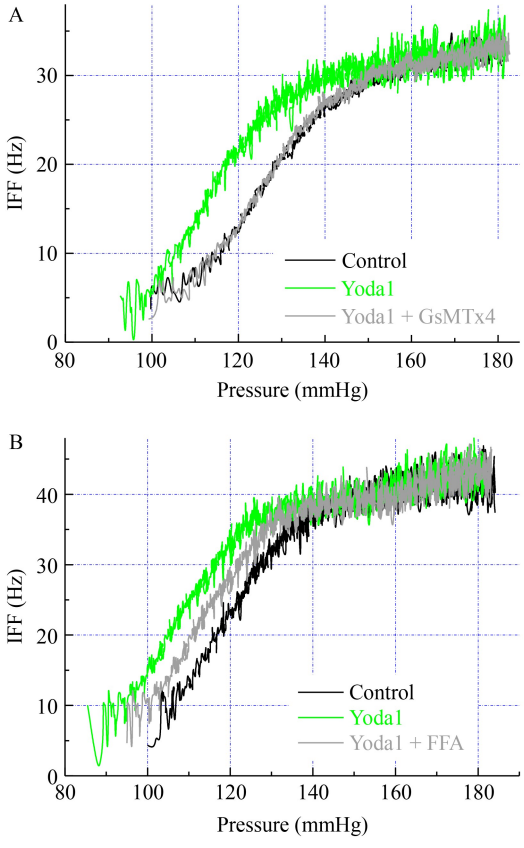

Fig. 2 Yoda1-mediated *Piezo1* channel activation significantly enhances the IFF of identified myelinated A-type single-fiber discharge and inhibitory effect of FAA or GsMTx4. Under the same experimental conditions, the instantaneous discharges were obtained before and after treatments. (A) Representative recordings in the control (DMSO, black), in the presence of Yoda1 (3 μmol/L, green), and Yoda1 with GsMTx4 (3 μmol/L, gray). (B) Representative recordings in the control (DMSO, black), in the presence of Yoda1 (3 μmol/L, green), and Yoda1 with FFA (10 μmol/L, gray).

a similar experiment using 10 μmol/L FAA showed that Yoda1-induced IFF increase was only partially blocked (Fig. 2B), indicating that *Piezo1* and *TRPM4* function synergistically in modulating baroreflex afferent input. Together, these results provide direct electrophysiological evidence that both *Piezo1* and *TRPM4* channels cooperate to regulate baroreflex afferent neurotransmission, with *Piezo1* playing a dominant role in afferent sensitivity.

Functional role of major and minor sub-threshold depolarizations in the development of spontaneous discharge of APs

Aforementioned data sets regarding the single-fiber recording imply that both *Piezo1*/*TRPM4* activation play an essential and intrinsic role to initiate an A-type afferent neurotransmission by showing instantaneous discharge at baroreceptor terminals. Strikingly, these single-fiber discharges of A-fiber can be further altered by Yoda1, leading us to one remaining question whether this could be verified on the level of their cell bodies within the NG, which receive continuous afferent signals converted from blood pressure and raised from baroreceptor terminals responding to the stretch-mediated the wall tension. Based on this, we hypothesized that some myelinated A-type NG neurons may exhibit spontaneous AP firing, reflecting their *in vivo* behavior. To test this, NG neurons were isolated and their fiber-type was classified based on waveform characteristics of APs (Fig. S3A–S3C).

In our experience, obtaining APs from A-type neurons is more difficult than C-types due to their increased fragility during enzymatic isolation. Therefore, spontaneous discharges/firings are not often seen in the isolated A-type NG neurons. To overcome these technical limitations, the isolation procedures are carefully conducted and searching for A-types is immediately

focused while they are ready for patching. Interestingly, less than 10% of tested A-type neurons fired spontaneously at resting potential near or below −60 mV with various frequency along with a slight and slow depolarization approximately 3–5 mV during 10-min gap-free current-clamp recording (Fig. 3A). Notably, apart from these spontaneous discharges of APs, a significant number of major (~10 mV beyond the resting, blue arrowheads) or minor (~5 mV above the resting) sub-threshold depolarizations, termed as Ma-STPs or Mi-STPs, could be observed during the observation. Meanwhile, a functional connection between Mi-STPs and Ma-STPs was confirmed by looking into the waveforms from selected portions of the recording with a proper expansion of time scaling (Fig. 3A, orange squares). Clearly, there is no doubt that several Mi-STPs could be superimposed to depolarize membrane to the degree of Ma-STPs near the threshold (Fig. S4B and S4C, orange circles) to trigger spontaneous discharge of APs, suggesting the functional connection and key role of Mi-STPs and Ma-STPs in visceral afferent signal generation.

An intrinsic capability of TTX-S, *Piezo1*, and *TRPM4* channels activation in A-type baroreflex afferent neurotransmission

Previous studies have indicated that the TTX-S channel, the only Na^+ channels expressed in the cell bodies of myelinated A-type NG neurons [20,21] and a major Na^+ channel in A-type vagal/baroreflex afferents that is critical for AP initiation and conduction [7,8,22]. To verify this, 100 nmol/L TTX was microperfused for 30 s at the end of the recording (Fig. 3A) with continuous bath perfusion. Intriguingly, the membrane potential was hyperpolarized by nearly 10 mV with both spontaneous discharge of APs and STPs were blocked (Figs. 3A and S4A) at initial phase and gradually recovered with Mi-STPs (Fig. S4A, black arrowheads) at the first, consequently Ma-STPs (blue arrowhead), and eventually spontaneous APs after ending TTX application, indicating that TTX-S channel is the most important Na^+ channel being responsible for initiating all depolarized events at least in A-type NG neurons. To further test the role of *TRPM4* in this spontaneous depolarization events, its blocker of 10 μmol/L FAA was administrated via microperfusion during the first 2 min and strikingly, only spontaneous discharges of APs were blocked (Fig. 3B) for additional 3 min and then partially recovered, while the number of Ma-STPs seemed to be significantly increased, it was actually not because of Ma-STPs remained after APs being blocked, which could be well explained by nearly equal of total numbers of APs plus Ma-STPs during the entire recordings before and after treatment (Fig. 3A vs. Fig. 3B). Additionally, by adding

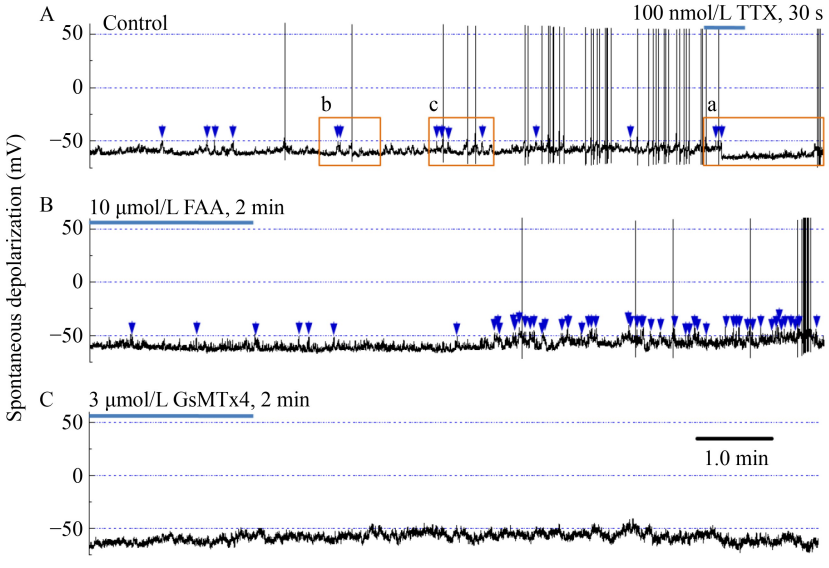

Fig. 3 Changes in spontaneous discharge of AP recorded from identified myelinated A-type neurons isolated from NG of adult male rats. A gap-free recording protocol was used to check spontaneous discharge of tested neurons under current-clamp configuration. The A-type neurons were initially determined by the waveform characteristics including AP firing threshold (APFT, lower than −40 mV), AP duration (APD_{50}, less than 1.0 ms) without a repolarization hump and finally confirmed by 100 nmol/L Cap (insensitive) applied at the end of recording. (A) Representative spontaneous AP discharges in the control condition. 100 nmol/L TTX was applied by microperfusion for 30 s at the end of this recording along with bath perfusion to minimize the effects on other neurons. (B) Representative spontaneous AP discharges and 10 μmol/L FAA was applied by microperfusion during the first 2 min with bath perfusion at meantime. (C) Representative spontaneous AP discharges and 3 μmol/L GsMTx4 was applied by microperfusion during the first 2 min with bath perfusion at meantime. The recordings were completed from the same patch, and the horizontal scale bar illustrated in (C) is applied for all panels. Blue arrowheads, major sub-threshold depolarization.

3 μmol/L GsMTx4 (Fig. 3C), spontaneous events disappeared without changing the resting membrane potential, suggesting that *Piezo1* activation plays an intrinsic role and has a pharmacological potential to modulate A-type visceral afferent functions compared with *TRPM4*. Most importantly, by deeply looking into the details (Fig. S4B and S4C, orange circled), several Mi-STPs could be superimposed to depolarize the membrane potential to the level of Ma-STPs near the threshold and then trigger repetitive discharges of APs. These data demonstrate the functional connection and the key role of these sub-threshold depolarizations in A-fibers/neurons afferent input generation, in which the roles of *Piezo1* and *TRPM4* is absolutely based upon availability of Na^+ channels.

Spontaneous inward currents behind the spontaneous depolarizations

From an electrophysiological point of view, any membrane depolarization must have corresponding inward currents to ensure the integrity of signals, therefore, a tremendous effort was put into practice to find A-type neurons with spontaneous inward currents and eventually 3 successful recordings were obtained from several dozen attempts by using gap-free voltage-clamp with −60 mV holding potential (Fig. 4A). Of noted, two magnitudes of inward currents were seen, and the current peaks for large group were all beyond 250 pA (Fig. 4B, red dash-dot line) ranging from nearly 260–500 pA (342 ± 47 pA) that are well equivalent to downward/depolarization portions of currents derivatives (Fig. S5) measured from the phase plots ranging 264–578 pA (377 ± 87 pA) generated from identified A-types evoked by a brief pulse (Fig. S3A–S3C, n = 23). While, the peaks of low grade of spontaneous inward currents were around 100 pA (52.7 ± 29.4 pA) and these were most likely to present the current derivatives of Ma-STPs (see the following). Additionally, an averaged frequency of these inward current events including both large and small magnitude was 16.4 ± 7.4 Hz, consistent with the total frequency of spontaneous depolarized events (Fig. 3).

Role of sub-threshold depolarizations in a majority of A-type NG neurons without spontaneous depolarization

Of noted, spontaneous depolarizing events were not detected in a majority of gap-free current-clamp recordings (Fig. 5A). This observation suggests that the tested A-type neurons may be from different visceral origin with significantly less afferent inputs and lower intrinsic power to fire spontaneously. As our expected, APs, Ma-STPs (Fig. 5B, blue arrowheads), and Mi-STPs (Fig. 5B, black arrowheads) were indeed observed in the presence of Yoda1. By looking into the details of current derivatives (Fig. 5C) with expansion and superimposition, more excitingly, the trajectory of either Mi-STPs or Ma-STPs looked like an AP taking off directly from the resting potential and showing similar depolarization, repolarization, and even after-hyperpolarization demonstrated by the current derivatives (Fig. 5E–5G). All these mentioned depolarized events disappeared with a

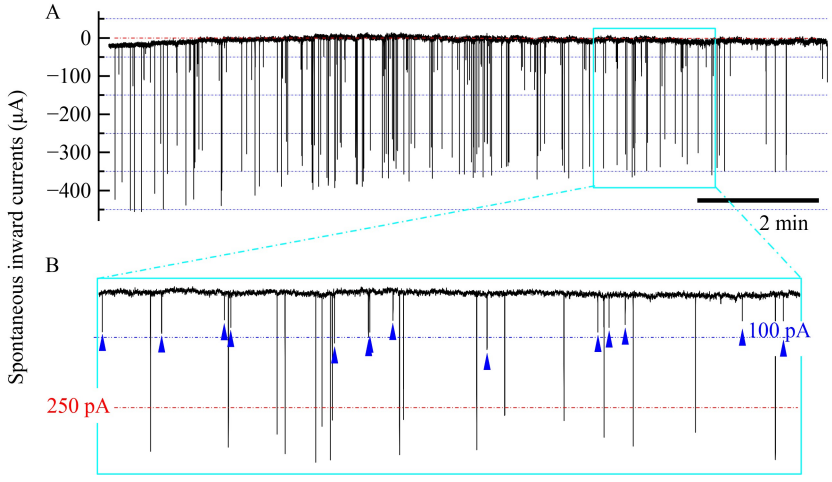

Fig. 4 Spontaneous inward currents recorded from identified A-type NG neurons using gap-free voltage-clamp. The holding potential for this voltage-clamp protocol was −60 mV and the duration of recording was at least 10 min. (A) Representative recording of spontaneous inward current. (B) The horizontal expansion of spontaneous events shown in (A, within squared part) from 480–600 s; blue or red short dash-dot line mean 100 pA or 250 pA, respectively; blue arrowheads mean small-grouped inward currents. The total number of events of entire recording (11 min) and within this 2 min was at least 184 and 31, respectively, corresponding to average frequencies of 16.58 Hz and 15.5 Hz. The representative example shown is from one A-type NG neuron.

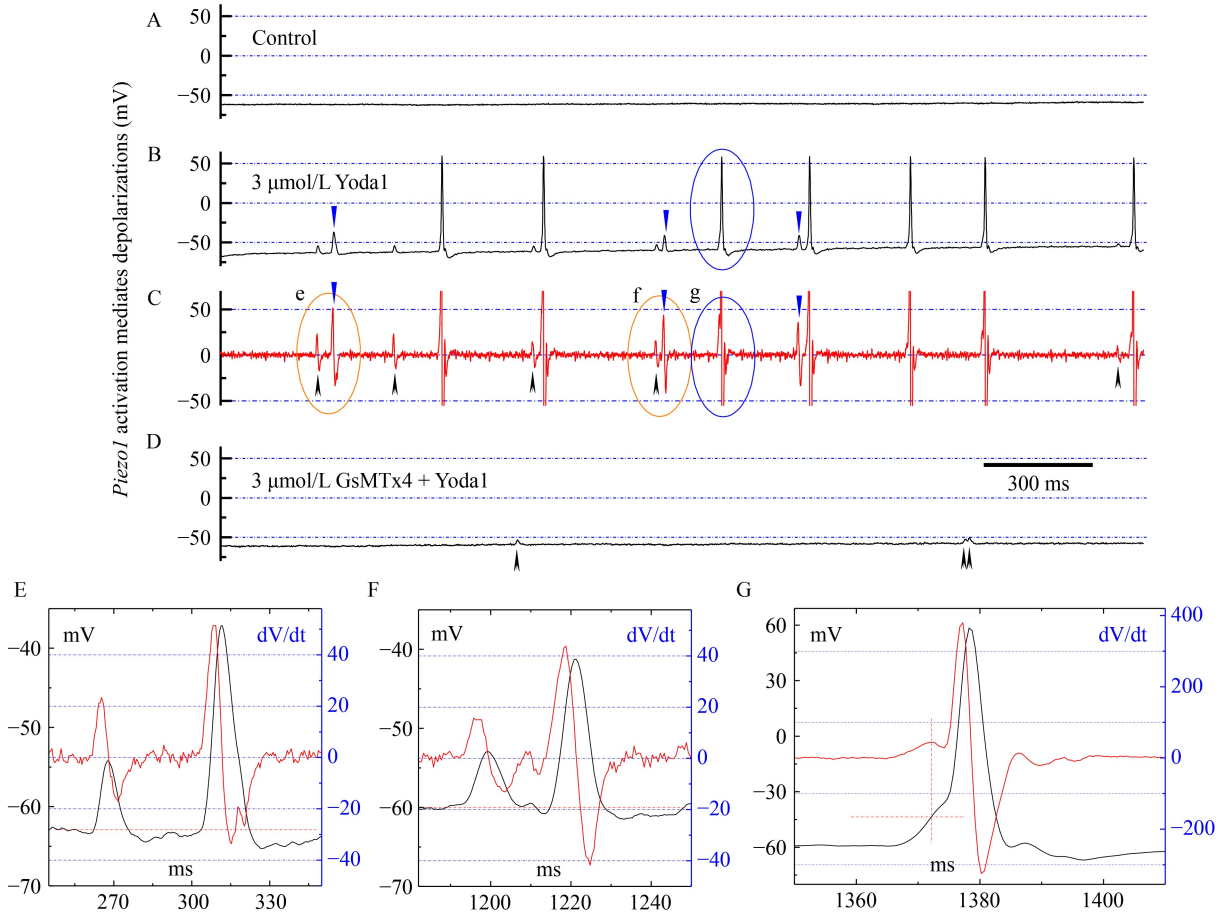

Fig. 5 *Piezo1* activation mediates all major (blue arrowheads), minor sub-threshold depolarizations (black arrowheads) and repetitive discharges of APs in identified A-type neurons. All representative recordings were obtained from the same patch using gap-free current-clamp protocol. (A, B) Recordings before and after application of 3 μmol/L Yoda1. (C) Current derivatives as a function of membrane voltage shown in (B). (D) Recording after 3 μmol/L GsMTx4 on top of Yoda1. (E, F) Horizontal and vertical expansion of parts of recordings circled in orange with labels shown in (C). (G) Horizontal expansion and superimposition of parts of recording circled as blue shown in (A) and (C) with labels. The scale bar in (D) is applied for all panels.

few Mi-STPs left in the presence of 3 μmol/L GsMTx4 on top of Yoda1 (Fig. 5D), reinforcing the critical role of *Piezo1*-mediated STPs in initiating baroreflex afferent signaling.

It is well known that the hump over the time course of repolarization is not present in the APs of A-type neurons identified from the slice (Fig. S2) and isolated preparation (Fig. S3), because it is a typical feature and commonly seen in the C-types (Fig. S6) due to reactivation of *Nav1.8* during the repolarization. However, the presence of a distinct repolarization hump observed in the Ma-STPs of this specific A-type neuron (Fig. 5E) remains unexplained based on current knowledge, warranting further investigation.

Pharmacological modulation of myelinated A-types neuroexcitation by *Piezo1*/*TRPM4* activation or inhibition

Yoda1-mediated neuroexcitation of a female-specific subpopulation of myelinated Ah-type neurons has recently been reported [2,23]. Here, we intended to focus on the regulatory effect of *Piezo1* activation on AP waveform characteristics and repetitive discharge profiles of A-types to assess its pharmacological potential beyond its intrinsic capability of baroreflex initiation. Extensive studies, including our own, have shown that A-type neurons are capable of firing APs at high frequencies, up to 50 Hz in isolated neurons, or 150 Hz in nodose slice preparations with vagal stimulation [22,23]. This suggests that these neurons encode a broad range of visceral afferent information, including baroreflex afferent signals, with significant intrinsic power mediated by *Piezo1*/*TRPM4* channels (Fig. 1). The ability to fire APs in the presence of a *Piezo1* agonist would be essential to scaling its pharmacological potential. For this regard, A-type neurons (n = 5 complete recordings) were identified (Fig. 6A and 6E) with relatively lower firing frequency within 1–10 Hz evoked by current depolarization steps before and after 3 μmol/L Yoda1 to assess the maximal

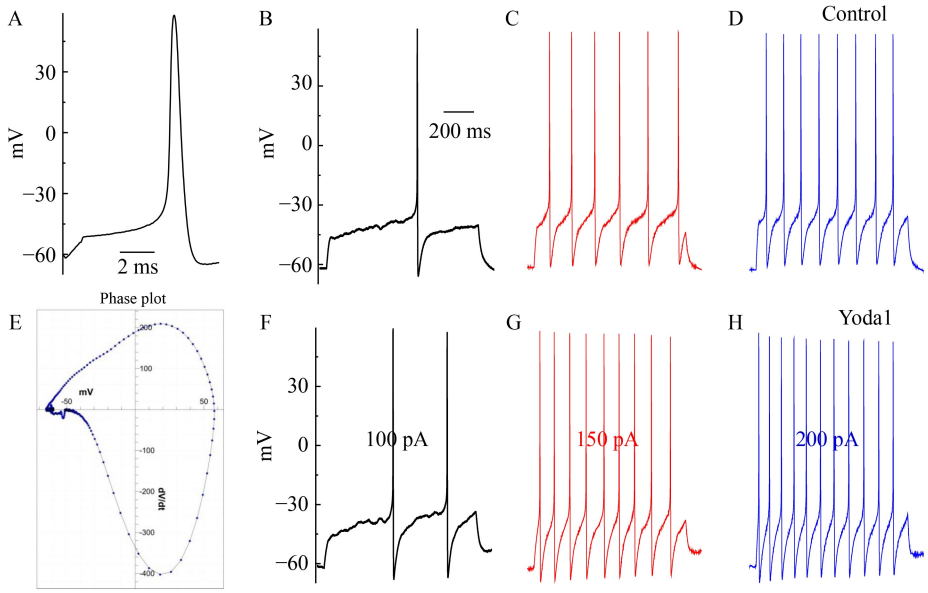

Fig. 6 Lower-frequency repetitive discharges evoked by depolarization steps in identified A-type neurons could be enhanced in the presence of 3 μmol/L Yoda1 under different stimulus intensities. Single and repetitive AP discharge were elicited by a brief pulse and step depolarization. (A, E) AP and phase plot to identify the A-type neurons. (B–D) Repetitive AP discharge elicited with 100, 150, and 200 pA steps before application of 3 μmol/L Yoda1. (F–H) Repetitive AP discharge elicited under identical step currents after application of 3 μmol/L Yoda1.

effect. Unlike myelinated Ah-types, the trajectory related AP parameters were not altered by Yoda1 (Data not shown). However, under same step-current conditions, the firing frequency particularly for this A-type was markedly increased by 100% at 100 pA, 50% at 150 pA, and 37.5% at 200 pA (Fig. 6F–6H), respectively, compared with the control condition (Fig. 6B–6D). These data suggest that *Piezo1* activation has a large scale of influence on evoked AP discharge with a reverse dependency upon the basal activity of tested neurons. Unfortunately, similar test was not conducted because a selective agonist for *TRPM4* channel is not available.

In addition, another group of identified A-type neurons (Fig. 7A, inset, n = 3 complete recordings) with a relatively higher firing frequency (30–50 Hz) evoked by a 200 pA current depolarization step (Fig. 7B) were selected to further test their intrinsic firing capability mediated by *Piezo1*/*TRPM4* channels. With 10 μmol/L FAA on board, the frequency evoked by identical current step was robustly reduced from 39 Hz fired through entire duration of protocol down to 19 Hz, with last AP not being evoked in the spike train (Fig. 7C), and further suppressed to 9 Hz bursting lasted only half protocol by adding 3 μmol/L GsMTx4 on top of FAA (Fig. 7D), suggesting a tremendously intrinsic power from both *Piezo1*/*TRPM4* channels under physiologic condition.

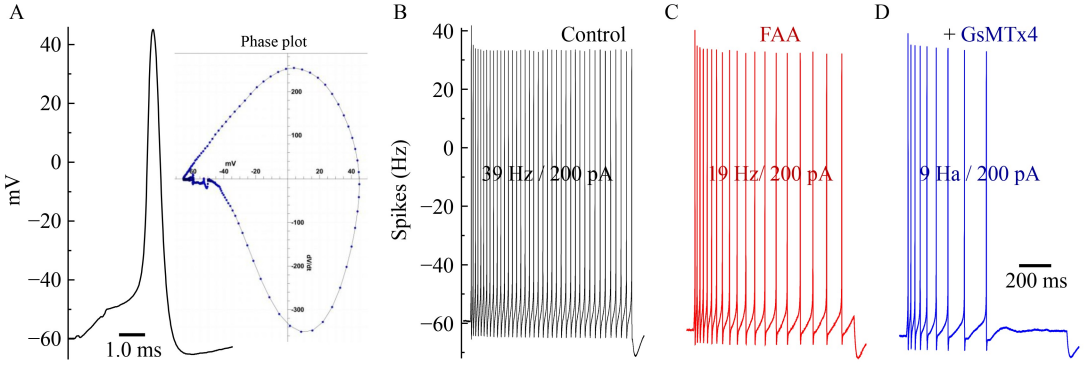

Fig. 7 High frequency repetitive discharge evoked by depolarization steps in identified A-type neurons could be reduced in the presence of GsMTx4 3 μmol/L. Single and repetitive AP discharges were elicited by a brief pulse and step depolarization. (A) A-type AP was identified by its waveform characteristics with phase plot (inset) and negative to 100 nmol/L capsaicin applied at the end of recording to double check the fiber-type. (B–D) Repetitive AP discharges before and after 10 mmol/L FAA or FAA plus 3 μmol/L GsMTx4 obtained from the same A-type neurons shown in (A) under an identical current step (200 pA). The horizontal scale shown in (D) is applied for all.

qRT-PCR detection and bioinformatics data analysis show a positive correlation the expression of *Piezo1* and *TRPM4*

Our aforementioned data sets clearly point out the functional distribution of both *Piezo1* and *TRPM4* channels in identified myelinated A-type fibers of the ADN and A-type neurons in the visceral/baroreflex afferent pathway. Therefore, to examine the tissue expression of these two channel genes, we collected NG tissue from adult male rats (n = 6) and performed qRT-PCR analysis (Fig. S8). The results showed that both channel genes were detectable in NG tissue, with similar expression levels. Given the presence of multiple types of NG neurons [17,18] and the use of adult male rats in this study, future single-cell qRT-PCR analysis [22] will be necessary to determine the distribution and expression profile of *Piezo1* and *TRPM4* in myelinated A-type neurons.

We downloaded single-cell RNA sequencing (scRNA-seq) data from the Tabula Sapiens database, focusing on the inferior olive nucleus in the medulla oblongata. We performed UMAP clustering of cell populations in the data set, with neurons labeled separately (Fig. 8A). The expression distribution of *TRPM4* and *PIEZO1* in neurons showed a similar pattern (Fig. 8B). Correlation analysis

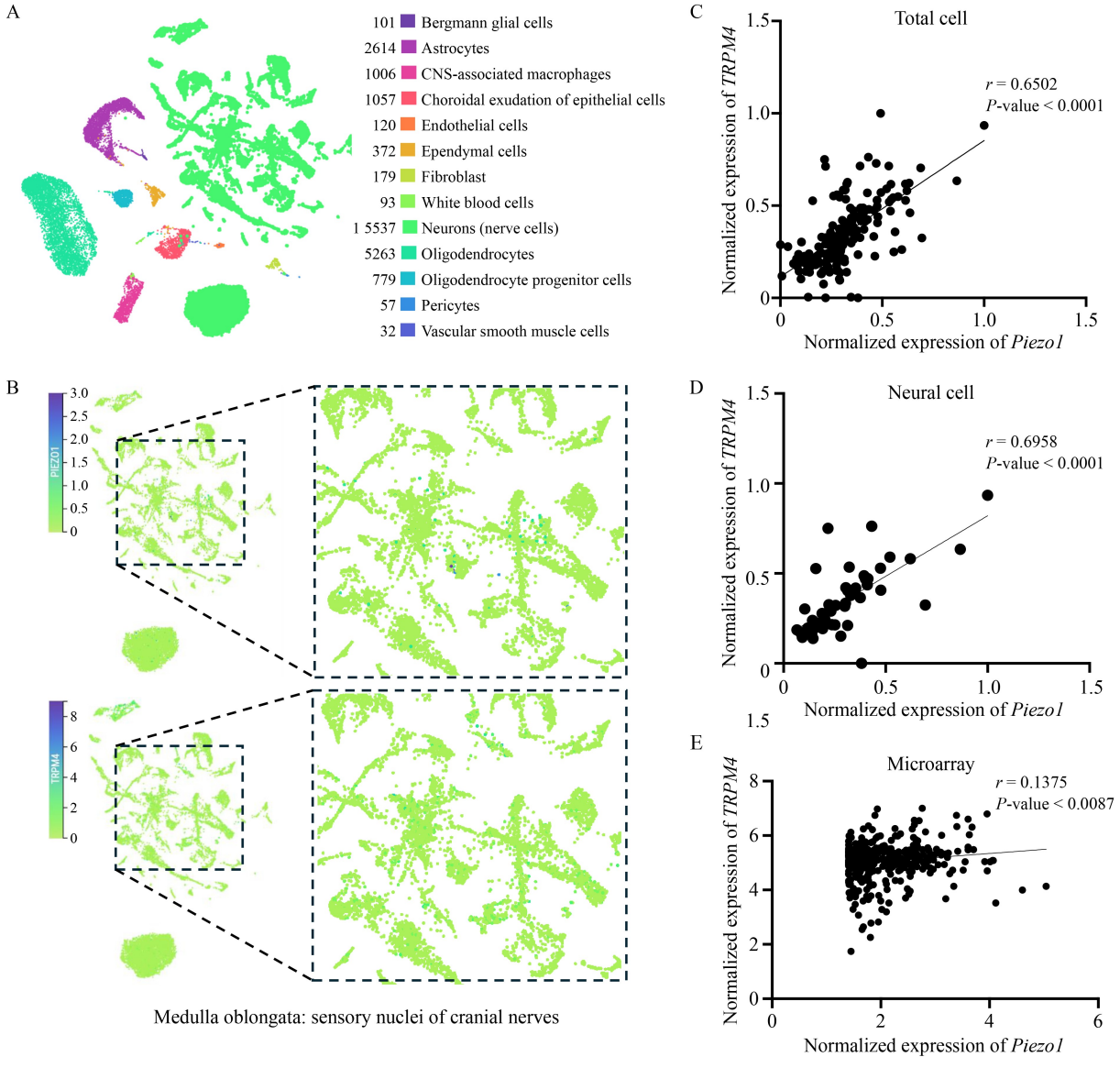

Fig. 8 Bioinformatics data showed a positive correlation between the expressions of *Piezo1* and *TRPM4*. (A) Single-cell sequencing data of medulla oblongata, focusing on the sensory nuclei of the cranial nerves in the medulla oblongata. (B) Single-cell sequencing data from neuronal cells showed consistency in the expression distribution of *Piezo1* and *TRPM4*. (C–E) Linear correlation pattern showed a positive relationship between the expression of *Piezo1* and *TRPM4* based on single-cell sequencing (for total cells and neural cells) and microarray data.

revealed a significant positive correlation between *TRPM4* and *Piezo1* expression across all cells and specifically within neurons (Fig. 8C and 8D). Analysis of GSE233733 (vagus nerve sequencing data from COVID-19 patients) and GSE43490 (vagus dorsal nucleus sequencing data) from the GEO database also showed a positive correlation between the expression of these two genes (Fig. 8E). Furthermore, we analyzed scRNA-seq data from the medulla-cerebellar nuclei-inferior olivary nucleus, which similarly demonstrated consistent co-expression of *TRPM4* and *Piezo1* (Fig. S8A and S8B). Additionally, sequencing data from the GEO database, including GSE233733 (vagus nerve RNA-seq from COVID-19 patients) and GSE43490 (dorsal motor nucleus of the vagus), further confirmed a significant correlation between the two genes (Fig. S8C and S8D). These findings suggest that *Piezo1* and *TRPM4* are co-expressed in NG neurons, particularly in myelinated A-type neurons, highlighting their potential functional interplay in the visceral/baroreflex afferent pathway.

Discussion

Baroreflex is an important mechanism by which the CNS controls blood pressure in response to acute fluctuations under physiological [1] and disease condition like hypertension [24,25] and some neurodegenerative disorders with orthostatic blood pressure changes [26,27]. The baroreflex is initiated by aortic baroreceptor (mechanoreceptors) and their mechanosensitive terminals could be activated by the wall-stretch-mediated mechanosensitive channel activation including *Piezols* [28], *TRPMs* [6] and TTX-S channels and further conversion of mechanical signals into the afferent neuronal signals that are encoded into trains of APs with different frequency upon the signals. Although this scientific conception of baroreflex has well been established, direct evidence are limited and those could be viewed under experimental/pharmacological conditions under functional and ion channel spectrum tested by single-fiber recording (aortic arch preparation) and whole-cell patch (vagus-nodose slice/isolated neuron preparations) from the terminals to the cell bodies.

Major findings of the current studys include: (1) TTX-S, *Piezo1*, and *TRPM4* channels are indispensable for initiation of baroreflex afferent inputs in identified A-fibers of ADN with an intrinsic capability and unique role of each; (2) this baroreflex afferent inputs could well be modulated by exogenous *Piezo1* agonist, suggesting the pharmacological potential of *Piezo1* activation in future perspective; nevertheless, due to lacking *TRPM4* agonist, the less role of *TRPM4* activation could only be predicted here upon the functional study with its blocker; (3) unlike *TRPM4*, *Piezo1* activation superimposes Ma-STPs to form major sub-threshold depolarization (Mi-STPs) near threshold, and triggers corresponding spontaneous/evoked APs of A-type neurons; (4) functional distribution of *Piezo1*/*TRPM4* channels are in line with their genes detection.

The advantages of the current investigation is that we could successfully record the single-fiber discharges in identified A-fibers without contaminated by C-fiber activity and vascular effect using our unique aortic arch preparation, notably, an IFF of this approach could well mimic the situation *in vivo* and the profiles of IFF could easily be viewed directly at the terminals; Additionally, A-type nodose neurons identified using vagus-nodose slice or isolated preparation have been well established allowing us further evaluating our data set collected from arch preparation at the cell bodies of A-fiber. However, some limitations for this investigation are not neglected, including (1) the lack of *TRPM4* agonist and its intrinsic capability and pharmacological impact being predicted only for now; (2) all data sets are collected from A-fiber or A-type nodose neurons, but fiber-specific distribution of these channels could not be explained by the expression at the tissue level, so future single-cell qRT-PCR detection is warranted; and (3) multi-types of afferent fibers within ADN or neurons housed in the nodose ganglia are verified, but the recordings are not collected from C-fibers in the current investigation, so it remains a question being answered if C-fibers play more dramatic roles in an initiation of baroreflex afferent neurotransmission simply because the numbers of C-fibers are > 80% of total ADN in adult male rats [18].

Strikingly, in this grouped A-type neurons (Fig. 3), spontaneous membrane depolarizations [8] manifested as APs firings with irregular interval, Ma-STPs, and Mi-STPs, so called a sub-threshold depolarizing hump in the central neurons [29], were clearly observed during the entire 10-min gap-free current-clamp protocol, and the dynamics of these spontaneous depolarized events were well consistent with the profiles of spontaneous inward currents. Apparently, all these spontaneous depolarized events are Tetrodotoxin-dependent, suggesting that TTX-S channels expressed in A-fiber or A-type neurons would be essential for initiating baroreflex/visceral afferent drives and maintain the resting by partial depolarization, which is supported by the fact that a small number of Na^+ channels within the activation window are never inactivated to retain a basal excitability [30]. So, without TTX-S currents, synergistic afferent initiation via *Piezo1*/*TRPM4* is absolutely impossible.

Further tests also notified that all spontaneous/evoked APs are fired on top of Ma-STPs superimposed from several Mi-STPs, and this superimposition could be triggered by low concentration of *Piezo1* activation (Fig. S7B). To clearly and directly show the connection between Ma-STPs and corresponded discharge, A-type AP was elicited by vagal stimulation in the slice

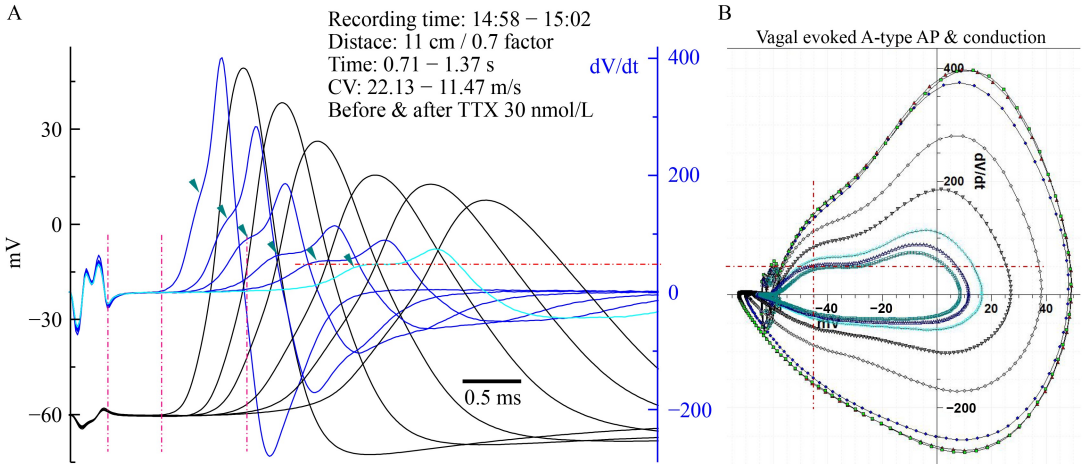

Fig. 9 Direct association between Ma-STPs and AP take off. A-type APs were elicited by vagal stimulation in the slice preparation before and after application of 30 nmol/L TTX. (A) Time-dependent reduction of CV, peak of AP, and current derivative; three vertical dash-dot lines from the left to the right: artifact of vagal stimulation, the time points of the 1st and the last AP taking-off, respectively; horizontal dash-dot line: the actual magnitude of Ma-STPs prior to the failure of AP. (B) The phase plots corresponded to each vagal-elicited AP, vertical dash-dot line: the time point for AP taking off on top of Ma-STPs, horizontal dash-dot line: the actual magnitude of Ma-STPs with TTX before the failure of AP generation.

preparation with very low concentration of TTX (30 nmol/L) on board so that a slower development of inhibition on CV and AP trajectory could be successfully recorded (Fig. 9A and 9B). Notably, the magnitude of depolarizing hump (dark cyan arrowheads) is gradually reduced down to its original height/Ma-STPs approximately 50 mV/ms (red horizontal dash-dot line) measured from the last successful AP and all corresponded current derivatives to their APs are developed on that platforms and TTX-S currents kick in at about −45 mV of this particular A-type (Fig. 9B, red vertical dash-dot line), which is equivalent well with the resting membrane potential of A-types. It is quite clear that measured current derivative and phase plot conjugated with AP elicited from isolated neurons/slice preparation with/without suitable agonist or antagonist would be a powerful tool for electrophysiological investigation.

Intriguingly, both spontaneous APs and Ma-STPs disappeared in the presence of GsMTx4, implying that *Piezo1* is another ion channel gates controlling the baroreflex afferent initiation. Clearly, *TRPM4* also contributes to intrinsic capability of baroreflex afferent neurotransmission [13,31] through the coupling mechanisms revealed by partially inhibition of both IFF of aortic arch and spontaneous/evoked APs from isolated preparations in the presence of FAA, indicating a synergetic role between *Piezo1* [32] and *TRPM4* [9]. Regarding Ma-STPs, our results are not consistent with the published literature [10] showing its *TRPM4*-dependency, which may be owing to the species and central location of *TRPM4*.

In addition, not only central but also peripheral integration of afferent inputs has been observed in both Ah- [33] and C-type [34] NG neurons by manipulation of trajectory of AP, especially the frequency-dependent widening of AP duration leading to more neurotransmitter release in the central location. However, this phenomenon is not detected in the A-types in the presence of Yoda1, but their firing frequency could be modulated on a large scale by *Piezo1* activation and inhibition, combined with their encoding capability, A-fibers/A-type neurons play a unique role in baroreflex/visceral afferent neurotransmission. From the pharmacological point of view, either change in intrinsic capability or modulation of firing frequency mediated by *Piezo1*/*TRPM4* channels activation/inhibition demonstrate a great potential and future perspective in the pharmacological convention.

Taken all these together, we have concluded that TTX-S, *Piezo1*, and *TRPM4* channels are multiple ionic passes to control and orchestrate an initiation of baroreflex afferent neurotransmission being directly and successfully evidenced from the baroreceptor terminals of A-fibers at aortic arch to the cell bodies of the 1st-order A-type nodose neurons.

Acknowledgements

This work was financially supported by the National Natural Science Foundation of China (Nos. 81971326 and 81573431) and partially supported by the Heilongjiang Provincial Research Institute Project (No. CZKYF2024-1-A003).

Compliance with ethics guidelines

Conflicts of interest Yinzhi Xu, Zhaoyuan Xu, Huixiao Fu, Mao

Yue, Jiaqun Li, Changpeng Cui, Xuelian Li, Xianghui Kong, and Baiyan Li declared that they have no conflict of interest.

All protocols for animals used in these experiments were consistent with the recommendations of the American Veterinary Medical Association Euthanasia Panel and the National Institutes of Health publication *Guide for the Care and Use of Laboratory Animals*, and approved by Harbin Medical University Institutional Animal Care and Use Committee.

Electronic supplementary material Supplementary material is available in the online version of this article at https://doi.org/10.1007/s11684-025-1167-x and is accessible for authorized users.

References

1. Ntalapera S, Miliotis P, Koskolo M, Donti O, Geladas N. Arterial blood pressure regulation during prolonged isometric exercise in artistic gymnastic athletes compared to controls. J Sports Med Phys Fitness 2025; 65(1): 140–147
2. Cui CP, Xiong X, Zhao JX, Fu DH, Zhang Y, Ma PB, Wu D, Li BY. Piezo1 channel activation facilitates baroreflex afferent neurotransmission with subsequent blood pressure reduction in control and hypertension rats. Acta Pharmacol Sin 2024; 45(1): 76–86
3. Ramirez-Navarro A, Lima-Silveira L, Glazebrook PA, Dantzler HA, Kline DD, Kunze DL. Kv2 channels contribute to neuronal activity within the vagal afferent-nTS reflex arc. Am J Physiol Cell Physiol 2024; 326(1): C74–C88
4. Andresen MC, Yang M. Dynamics of sensory afferent synaptic transmission in aortic baroreceptor regions on nucleus tractus solitarius. J Neurophysiol 1995; 74(4): 1518–1528
5. Andresen MC, Kunze DL. Nucleus tractus solitarius–gateway to neural circulatory control. Annu Rev Physiol 1994; 56(1): 93–116
6. Uchida K. TRPM3, TRPM4, and TRPM5 as thermo-sensitive channels. J Physiol Sci 2024; 74(1): 43
7. Nair SS, Pavelkova N, Murphy CM, Kollarik M, Taylor-Clark TE. Action potential conduction in the mouse and rat vagus nerve is dependent on multiple voltage-gated sodium channels (Na(V)1s). J Neurophysiol 2023; 130(3): 684–693
8. Nascimento AI, Da Silva TF, Fernandes EC, Luz LL, Mar FM, Safronov BV, Sousa MM. Sensory neurons have an axon initial segment that initiates spontaneous activity in neuropathic pain. Brain 2022; 145(5): 1632–1640
9. Guo Y, Cheng D, Yu ZY, Schiatti T, Chen AY, Hill AP, Peyronnet R, Feneley MP, Cox CD, Martinac B. Functional coupling between Piezo1 and TRPM4 influences the electrical activity of HL-1 atrial myocytes. J Physiol 2024; 602(18): 4363–4386
10. Li K, Abbott SBG, Shi Y, Eggan P, Gonye EC, Bayliss DA. TRPM4 mediates a subthreshold membrane potential oscillation in respiratory chemoreceptor neurons that drives pacemaker firing and breathing. Cell Rep 2021; 34(5): 108714
11. Sims R, Bendifallah I, Grimm C, Lafirdeen ASM, Domínguez S, Chan CY, Lu X, Forget BC, St-Pierre F, Papagiakoumou E, Emiliani V. Scanless two-photon voltage imaging. Nat Commun 2024; 15(1): 5095
12. Tang H, Hao R, Ma D, Yao Y, Ding C, Zhang X, Zhang A. Structural modification and pharmacological evaluation of (thiadiazol-2-yl)pyrazines as novel piezo1 agonists for the intervention of disuse osteoporosis. J Med Chem 2024; 67(21): 19837–19851
13. Binkle-Ladisch L, Pironet A, Zaliani A, Alcouffe A, Mensching D, Haferkamp U, Willing A, Woo MS, Erdmann A, Jessen T, Hess SD, Gribbon P, Pless O, Vennekens R, Friese MA. Identification and development of TRPM4 antagonists to counteract neuronal excitotoxicity. iScience 2024; 27(12): 111425
14. Wladyka L, Feng B, Glazebrook PA, Schild JH, Kunze DL. The KCNQ/M-current modulates arterial baroreceptor function at the sensory terminal in rats. J Physiol 2008; 586(3): 795–802
15. Feng B, Li BY, Nauman EA, Schild JH. Theoretical and electrophysiological evidence for axial loading about aortic baroreceptor nerve terminals in rats. Am J Physiol Heart Circ Physiol 2007; 293(6): H3659–H3672
16. Li BY, Schild JH. Patch clamp electrophysiology in nodose ganglia of adult rat. J Neurosci Methods 2002; 115(2): 157–167
17. Li BY, Schild JH. Electrophysiological and pharmacological validation of vagal afferent fiber type of neurons enzymatically isolated from rat nodose ganglia. J Neurosci Methods 2007; 164(1): 75–85
18. Li BY, Qiao GF, Feng B, Zhao RB, Lu YJ, Schild JH. Electrophysiological and neuroanatomical evidence of sexual dimorphism in aortic baroreceptor and vagal afferents in rat. Am J Physiol Regul Integr Comp Physiol 2008; 295(4): R1301–R1310
19. Santa Cruz Chavez GC, Li BY, Glazebrook PA, Kunze DL, Schild JH. An afferent explanation for sexual dimorphism in the aortic baroreflex of rat. Am J Physiol Heart Circ Physiol 2014; 307(6): H910–H921
20. Schild JH, Kunze DL. Differential distribution of voltage-gated channels in myelinated and unmyelinated baroreceptor afferents. Auton Neurosci 2012; 172(1–2): 4–12
21. Schild JH, Kunze DL. Experimental and modeling study of Na^+ current heterogeneity in rat nodose neurons and its impact on neuronal discharge. J Neurophysiol 1997; 78(6): 3198–3209
22. Hadley S, Pati MJ, Pavelkova N, Kollarik M, Taylor-Clark TE. Contribution of tetrodotoxin-sensitive, voltage-gated sodium channels (Na(V)1) to action potential discharge from mouse esophageal tension mechanoreceptors. Am J Physiol Regul Integr Comp Physiol 2021; 321(5): R672–R686
23. Xu YZ, Xu ZY, Fu HX, Yue M, Li JQ, Cui CP, Wu D, Li BY. Caution for multidrug therapy: significant baroreflex afferent neuroexcitation coordinated by multi-channels/pumps under the threshold concentration of Yoda1 and dobutamine combination. Biomolecules 2024; 14(10): 1311
24. Flôr AFL, Duarte-Maia S, Fernandes-Costa F, Pessoa de Souza RM, Braga VA, Amaral SL, Mascarenhas SR, Brito-Alves JL, Colombari DSA, Cruz JC. Chronic cannabidiol treatment induces cardiovascular improvement in renovascular hypertensive rats. J Hypertens 2025; 43(1): 98–108
25. Ma Y, Zhang Y, Hamaya R, Westerhof BE, Shaltout HA, Kavousi M, Mattace-Raso F, Hofman A, Wolters FJ, Lipsitz LA, Ikram MA. Baroreflex sensitivity and long-term dementia risk in older adults. Hypertension 2025; 82(2): 347–356
26. Okkels N, Horsager J, Fedorova TD, Knudsen K, Skjærbæk C, Andersen KB, Labrador-Espinosa M, Vestergaard K, Mortensen JK, Klit H, Møller M, Danielsen EH, Johnsen EL, Bekan G,

Hansen KV, Munk OL, Damholdt MF, Kjeldsen PL, Hansen AK, Gottrup H, Grothe MJ, Borghammer P. Impaired cholinergic integrity of the colon and pancreas in dementia with Lewy bodies. Brain 2024; 147(1): 255–266

27. Choi S, Kim R, Kang N, Byun K, Park K, Jun JS. eKim R, Kang N, Byun K, Park K, Jun JS. Associations of orthostatic hypotension and orthostatic intolerance with domain-specific cognitive decline in patients with early parkinson disease: an 8-year follow-up. J Am Med Dir Assoc 2024; 25(5): 866–870
28. Baumer-Harrison C, Elsaafien K, Johnson DN, Aponte JDP, de Araujo A, Patel S, Bruce EB, Harden SW, Frazier KA, de Lartigue G, Krause EG, de Kloet AD. Alleviating hypertension by selectively targeting angiotensin receptor-expressing vagal sensory neurons. J Neurosci 2024; 44(9): e1154232023
29. Armstrong WE, Stern JE. Electrophysiological and morphological characteristics of neurons in perinuclear zone of supraoptic nucleus. J Neurophysiol 1997; 78(5): 2427–2437
30. Tikhonova TB, Sharkov AA, Zhorov BS, Vassilevski AA. Diverse biophysical mechanisms in voltage-gated sodium channel Na(v)1.4 variants associated with myotonia. FASEB J 2024; 38(16): e23883
31. O'Malley JJ, Seibt F, Chin J, Beierlein M. TRPM4 conductances in thalamic reticular nucleus neurons generate persistent firing during slow oscillations. J Neurosci 2020; 40(25): 4813–4823
32. Stocker SD, Sved AF, Andresen MC. Missing pieces of the Piezo1/Piezo2 baroreceptor hypothesis: an autonomic perspective. J Neurophysiol 2019; 122(3): 1207–1212
33. Liu Y, Wen X, Liu SZ, Song DX, Wu D, Guan J, Wang LQ, Li JN, Lu XL, Guo TZ, Zuo CM, Qiao GF, Li BY. KCa1.1-mediated frequency-dependent central and peripheral neuromodulation via Ah-type baroreceptor neurons located within nodose ganglia and nucleus of solitary tract of female rats. Int J Cardiol 2015; 185: 84–87
34. Li BY, Feng B, Tsu HY, Schild JH. Unmyelinated visceral afferents exhibit frequency dependent action potential broadening while myelinated visceral afferents do not. Neurosci Lett 2007; 421(1): 62–66